Journal of Magnetic Resonance **157,** 82–91 (2002)
doi:10.1006/jmre.2002.2577

Categories of Coherence Pathways for the CPMG Sequence

Y.-Q. Song

Schlumberger-Doll Research, 36 Old Quarry Road, Ridgefield, Connecticut 06877

E-mail: ysong@slb.com

Received January 28, 2002; revised May 20, 2002

The CPMG sequence has been extremely useful for efficient measurements of NMR signal, spin–spin relaxation, and diffusion, particularly in inhomogeneous magnetic fields, such as when samples are outside the magnet and RF coil. Due to the inaccuracy of the pulses and the off-resonance effects, the CPMG echoes have contributions from the Hahn echo as well as signals that are similar to stimulated echoes. The systematic understanding of the CPMG pulse sequence requires decomposing the magnetization dynamics into different coherence pathways. In this paper, we describe a method to classify the CPMG coherence pathways and illustrate the nature of these types of pathways. This classification shows that direct echo and stimulated echoes are the major contribution to the CPMG signal. It also provides a clear understanding of the effect of restricted diffusion in porous media.

Key Words: **CPMG; coherence pathway; off-resonance effects; diffusion; restricted diffusion.**

I. INTRODUCTION

The CPMG sequence (*1, 2*) is remarkable in producing a long train of echo signals that enables efficient measurements of spin–spin relaxation and the diffusion constant, as well as maximizing signal-to-noise ratio in various challenging experimental conditions (*3–5*). When the resonance linewidth is much less than the RF field strength, ω_1, the π pulses can be effective 180 degree rotations of magnetization to refocus the magnetic field inhomogeneity at each echo time. This is the direct echo pathway. When the pulses are inaccurate or the linewidth is comparable to ω_1, there will be a finite probability for the magnetization to remain unchanged or rotated to the longitudinal direction (*6*). In general, many coherence pathways (*7*) contribute to the CPMG echo signals and the number of pathways grow exponentially as a function of the echo number (N), $\sim 3^N$. The effects of an inhomogeneous field on the CPMG sequence have been researched for CPMG echoes (*8–12*). Goelman and Prammer (*8*) have partitioned the coherence pathways into direct echo and indirect echoes and simulate the echo signals using a subset of the coherence pathways that are most important. Hürlimann (*12*) has presented a thorough analysis of all coherences and diffusion effects. For example, the 15th echo has about 10^6 coherence pathways and the 50th echo has 10^{24}. Thus, it is difficult to extend such calculation to high echo numbers due to the enormously large number of coherence pathways. Furthermore, such formalism is developed for unrestricted diffusion. For restricted diffusion when the mean squared displacement is no longer proportional to time, each coherence pathway has to be reexamined (*13–15*). For example, the diffusion constant can be dependent on the diffusion time and it is unclear what diffusion constant should be used to analyze the CPMG echo decay in porous media.

The current paper presents a classification of the coherence pathways of CPMG and the diffusion effects in constant magnetic field gradient (*7, 8, 12*). We show that only a fraction of the total number of pathways have a major contribution to the CPMG echoes. These coherence pathways are characterized by a combination of segments like stimulated echo and spin echo (*16*). This allows us to obtain the spectrum and the diffusion decay rates of large-N echoes. Using this classification, we have identified the diffusion time for all coherence pathways and found that it is appropriate to use the short-time diffusion constant to describe the CPMG echo decay due to restricted diffusion.

II. BRIEF REVIEW OF CPMG COHERENCE PATHWAYS

We follow the notations used in Ref. (*12*) in defining three states of spin magnetization of an ensemble of spin-1/2 nuclei, M_0, M_-, and M_+:

$$\begin{aligned} M_0 &= M_z, \\ M_+ &= M_x + iM_y \\ M_- &= M_x - iM_y. \end{aligned} \qquad [1]$$

These states are marked by q which can be 0, +1, and −1 (or 0, +, and −), respectively. The magnetization vector, **M**, is expressed using the bases of M_0, M_-, and M_+. We denote the rotation of the magnetization due to a RF pulse by a matrix, **R**,

$$\mathbf{M}(t_p) = \mathbf{R} \cdot \mathbf{M}(0). \qquad [2]$$

Here, $\mathbf{M}(0)$ and $\mathbf{M}(t_p)$ are the magnetization vectors before and after the pulse and the pulse duration is t_p. **R** depends

1090-7807/02 $35.00

on the Larmor frequency offset from the RF frequency ω_{RF}, $\Delta\omega_0 \equiv \gamma|B_0| - \omega_{RF}$, ω_1, and t_p. Then, the nutation frequency is $\Omega \equiv \sqrt{\omega_1^2 + \Delta\omega_0^2}$ where $\omega_1 = \gamma B_1/2$, and the tipping angle is Ωt_p. The matrix elements, $R_{l,m}$, are given in Ref. (*12*) and repeated here

$$\begin{aligned} R_{+,+} &= R^*_{-,-} \\ &= \frac{1}{2}\left\{\left(\frac{\omega_1}{\Omega}\right) + \left[1 + \left(\frac{\Delta\omega_0}{\Omega}\right)^2\right]\cos(\Omega t_p)\right\} \\ &\quad + i\left(\frac{\Delta\omega_0}{\Omega}\right)\sin(\Omega t_p) \end{aligned} \quad [3]$$

$$R_{0,0} = \left(\frac{\Delta\omega_0}{\Omega}\right)^2 + \left(\frac{\omega_1}{\Omega}\right)^2 \cos(\Omega t_p) \quad [4]$$

$$\begin{aligned} R_{+,0} &= R^*_{-,0} \\ &= \frac{\omega_1}{\Omega}\left\{\frac{\Delta\Omega_0}{\Omega}[1 - \cos(\Omega t_p)] - i\sin(\Omega t_p)\right\} e^{+i\varphi} \end{aligned} \quad [5]$$

$$\begin{aligned} R_{0,+} &= R^*_{0,-} \\ &= \frac{\omega_1}{\Omega}\left\{\frac{\Delta\Omega_0}{\Omega}[1 - \cos(\Omega t_p)] - i\sin(\Omega t_p)\right\} e^{-i\varphi} \end{aligned} \quad [6]$$

$$\begin{aligned} R_{+,-} &= R^*_{-,+} \\ &= \frac{1}{2}\left(\frac{\omega_1}{\Omega}\right)^2 [1 - \cos(\Omega t_p)] e^{+i2\varphi}. \end{aligned} \quad [7]$$

φ is the phase of the pulse. In this paper, we consider the CPMG sequence and thus encounter two rotations for the $\pi/2$ and π pulses. We will note the matrices by $L_{q,q'}$ for the $\pi/2$ pulse and $\Lambda_{q,q'}$ for the π pulse.

We label the magnetization state between the π pulse k and $k+1$ by q_k, which can be 0, $+1$, and -1. A coherence pathway for the Nth echo is characterized by a series of $N+1$ numbers, $q_0, q_1, q_2, \ldots, q_N$. For the Nth echo, q_N should be $+1$ since the transverse magnetization is to be detected. q_0 is the coherence after the initial $\pi/2$ pulse, and it can be $+$ or $-$ selected by the usual phase cycling of the $\pi/2$ pulse. The contribution of a coherence pathway to the magnetization of the Nth echo, in the absence of relaxation and diffusion, is

$$\frac{M_{q_0,q_1,\ldots,q_N}}{M_0} = \left(L_{0,q_0}\prod_{k=1}^{N}\Lambda_{q_k,q_{k-1}}\right)\exp\left(i\,\Delta\omega_0\sum_{k=0}^{N} q_k t_k\right), \quad [8]$$

where M_0 is the equilibrium magnetization. An echo occurs when the phase factor becomes zero,

$$\sum_{k=0}^{N} q_k t_k = 0, \quad [9]$$

where t_k is the time duration between pulse k and $k+1$. The observed echo M is a sum of all coherence pathways.

The effects of spin–spin and spin–lattice relaxation can be readily incorporated into the above formula by a multiplicative factor,

$$\exp\left[-\sum_{k=1}^{N}\left(q_k^2/T_2 + \frac{1-q_k^2}{T_1}\right)t_k\right], \quad [10]$$

since T_1 and T_2 are effective when q_k is 1 or 0, respectively. The effect of diffusion introduces an extra factor in Eq. [8],

$$\left\langle \exp\left(i\sum_{k=0}^{N} q_k\phi_k\right)\right\rangle. \quad [11]$$

Here, ϕ_k is the random phase factor due to diffusion between pulse k and $k+1$ in the presence of magnetic field gradients. The angle brackets $\langle\ldots\rangle$ represent an ensemble average of the random phase factors, $\phi_0, \phi_1, \phi_2, \ldots, \phi_N$. For unrestricted diffusion in a constant field gradient g, this contribution can be written as (*12, 17*)

$$\left\langle \exp\left(i\sum_{k=1}^{N} q_k\phi_k\right)\right\rangle \equiv \exp\left(-\eta_{Q_N}\gamma^2 g^2 D t_e^3 N\right), \quad [12]$$

where Q_N denotes a coherence pathway for the Nth echo and η_{Q_N} is the normalized diffusion decay rate. γ is the gyromagnetic ratio and D is the diffusion constant. Hürlimann has calculated η_{Q_N} of all coherence pathways for early echoes (*12*) by finding all Q_N's. In this paper, we will classify the coherence pathways by a series of segments, for instance, direct echo, i.e., $+-$, singly stimulated echo, i.e., $-0+$, and triply stimulated segment, i.e., $--00++$. Such classification will allow more rapid calculation of η and thus extend the analysis of CPMG echoes to much larger N. Also important, this classification will be useful to understand the effects of restricted diffusion.

Table 1 shows a list of all coherence pathways for the fifth echo and the corresponding η for each coherence pathway ordered by the value of ηN. Within each class, all coherence pathways have the same amplitude. Several interesting observations can be made from Table 1. First, permutations of zeros and the corresponding rearrangement of $+-$ and $-+$ segments in a coherence pathway do not change η_{Q_N}, for example, classes 1–7. In fact, some of the permutations are completely degenerate with identical amplitude, such as just changing the positions of $+0-$ within class 2. However, a change from two $-0+$ segments to one $-00+$ segment will cause a sign change in the amplitude, classes 3 and 4, although the decay rate remains. Second, the presence of zeros increases ηN by 2 for each "0" in the coherence pathways in classes 1–7. Third, the presence of one $++--$ segment increases ηN by 24 and a $+++---$ increases ηN by 120.

TABLE 1
All Coherence Pathways for the Fifth Echo

Class	$N\eta$	n_Q	Coherence pathway : $q_0q_1q_2q_3q_4q_5$
1	5	1	$-+-+-+$
2	7	4	$+0-+-+,\ +-0+-+,$ $+-+0-+,\ +-+-0+$
3	9	3	$-00+-+,\ -+00-+,\ -+-00+$
4	9	3	$-0+0-+,\ -0+-0+,\ -+0-0+$
5	11	2	$+-000+,\ +000-+$
6	11	2	$+0-00+,\ +00-0+$
7	13	1	$-0000+$
8	29	3	$-++--+,\ -+--++,\ --++-+$
9	31	6	$++--0+,\ +--+0+,\ ++-0-+,$ $+-0-++,\ +0+--+,\ +0--++$
10	33	3	$--+00+,\ -0-+0+,\ -00-++$
11	53	1	$--+-++$
12	55	2	$+--0++,\ ++0--+$
13	57	2	$--0+0+,\ -0-0++$
14	81	1	$--00++$
15	125	1	$---+++$

Note. $\eta_Q N$ is the decay factor; n_Q is the number of permutations with the same $\eta_Q N$. Within each class, all coherence pathways have the same amplitude. Note that from class 7 to 8, there is a jump in $N\eta$ due to the presence of $++--$ in the coherence pathways.

III. CATEGORIES OF COHERENCE PATHWAYS

The above observation provides a motivation for the following classification of coherence pathways based on their contribution to $N\eta$.

A. Direct Echo

This is the simplest class of coherence segments, characterized by the alternating $+$ and $-$,

$$+- \qquad \text{and} \qquad -+. \tag{13}$$

The amplitude of this coherence segment is given by

$$\Lambda_{+,-}. \tag{14}$$

With this segment alone, an entire echo train can be constructed:

$$q_0\underbrace{\cdots-+\cdots-+}_{N}. \tag{15}$$

From Eq. [9], q_0 is determined to be $-$ when N is odd, and $+$ when N is even. It is named the direct echo in reference to the original idea of spin echo by Hahn that the role of the π pulses is to invert the magnetization (*16*) and changing the coherence from $-$ to $+$ or $+$ to $-$. The diffusion-induced phases ϕ_k's cancel each other between the adjacent intervals over a time period on the order of t_E. Because of this cancelation over the shortest time interval, this coherence pathway decays the slowest among all pathways. This pathway can be the predominant one for the on-resonance signal with perfect π pulses. This can be seen from the matrix elements, Eq. [7], that $\Lambda_{+,-}=1$ for $\Delta\omega=0$ and $\omega_1 t_p=\pi$. However, in most experimental conditions, it is nevertheless difficult to maintain $\omega_1 t_p=\pi$ for the entire sample volume. Thus, for large echo numbers, the contribution from the direct echo will invariably decay. Furthermore, the off-resonance amplitude of direct echo is generally reduced from the on-resonance signal and it also decays due to the less than unity of the matrix elements. We will discuss the echo spectrum and the effects of nonideal pulses later.

B. Singly Stimulated Echoes

This class is very similar to the stimulated echo also described by Hahn (*16*). The basic segments are formed by a $-$ and a $+$ separated by a few 0's,

$$-\underbrace{0\cdots0}_{s_1}+, \qquad \text{and} \qquad +\underbrace{0\cdots0}_{s_1}-, \tag{16}$$

where s_1 is the number of zeros between the $+$ and $-$. To form a complete coherence pathway for the Nth echo, one may have n_{s_1} number of such segments as well as segments with other s_1. The total number of 0's would be $N_1=\sum_{s_1} s_1 n_{s_1}$. Then, $(N-N_1)/2$ number of direct echo segments, $+-$ or $-+$ are to be included. Again, q_0 can be determined by using Eq. [9]. The amplitude of one of such coherence segments is given by

$$\Lambda_{+,0}{\Lambda_{0,0}}^{s_1-1}\Lambda_{0,-}. \tag{17}$$

The diffusion factor ηN is given by

$$\eta N=(3N_1+1)+(N-N_1-1)=N+2N_1. \tag{18}$$

The term $3N_1+1$ corresponds to the stimulated segment and the second term $N-N_1-1$ is due to the direct echo segments. This result can be easily understood by comparing to the diffusion decay in a stimulated echo experiment (*16*) using pulsed field gradients (*18*). In a stimulated echo experiment, three $\pi/2$ pulses are used:

$$\pi/2-\delta-\pi/2-\Delta-\pi/2-\delta-echo. \tag{19}$$

During the two time periods of δ, a pulsed field gradient g is applied. It has been shown (*16*) that the decay factor due to diffusion is

$$\exp\left[-D\gamma^2g^2\delta^2\left(\Delta+\frac{2}{3}\delta\right)\right]. \tag{20}$$

The coherence pathway in the stimulated echo sequence is identical to the stimulated segment in CPMG. In the case of CPMG,

$\delta = t_e/2$, $\Delta = s_1 t_e$. Thus, the decay during the stimulated segment is $3N_1 + 1$. Including the direct echo segment, it is straightforward to arrive at Eq. [18].

The exponent in Eq. [20] is often rewritten in terms of the mean-square displacement ($\langle r^2 \rangle$) of the diffusing molecules at a diffusion time $\Delta + 2\delta/3$ (*19, 20*):

$$-(\gamma g \delta)^2 \langle r^2 \rangle / 6. \qquad [21]$$

This expression illustrates an important understanding of the stimulated echo sequence and also the stimulated segment in CPMG that the attenuation is a measure of the net diffusion displacement between the time period from the beginning to the end of the sequence, irrespective of the trajectories that a molecule may experience (*19*). Thus, this expression (Eq. [21]) is valid for restricted diffusion or any other forms of molecular dynamics provided $(\gamma g \delta)^2 \langle r^2 \rangle / 6 \ll 1$. Using this argument, we observe that the diffusion time for a direct echo segment is $t_e/3$ [21] which is the shortest time scale in the pulse sequence. On the other hand, the stimulated echo pathways can measure diffusion over a much longer time, $s_1 t_e$.

C. Triple Echoes

The basic segment of a triple echo is similar to the direct echo in that the magnetization remains in the transverse plane and it involves only + and −,

$$++--, \qquad \text{and} \qquad --++. \qquad [22]$$

The amplitude of this segment is given by

$$\Lambda_{+,+}\Lambda_{+,-}\Lambda_{-,-} \qquad [23]$$

The diffusion decay contribution of this segment can be calculated from the Hahn formula for direct echo taken into account the effectively tripled precession time,

$$\frac{1}{12} D(\gamma g)^2 (3t_e)^3 = \frac{1}{12} D(\gamma g)^2 (t_e)^3 \times 27. \qquad [24]$$

For a segment of time $3t_e$ formed by direct echo segments, the decay would have been $\frac{1}{12} D(\gamma g)^2 (t_e)^3 \times 3$, thus making the contribution of the triple echo a factor of 24 (=27 − 3) more than the direct echo segments.

D. Triply Stimulated Echoes

This class has several subclasses depending on where the 0's are inserted into the triple echo segment.

- This subclass follows the form of the singly stimulated segments except starting and ending with ++ and −−:

$$++\underbrace{0\cdots0}_{s_3}--, \qquad \text{and} \qquad --\underbrace{0\cdots0}_{s_3}++. \qquad [25]$$

The amplitude of this segment is

$$\Lambda_{+,+}\Lambda_{+,0}\Lambda_{0,0}{}^{s_3-1}\Lambda_{0,-}\Lambda_{-,-}. \qquad [26]$$

It is straightforward to calculate the additional diffusion decay during this segment compared to the triple echo of $26 s_3$.

- The second subclass is in fact a singly stimulated segment imbedded in a triple echo segment,

$$--+\underbrace{0\cdots0}_{s_3}+, \qquad \text{and} \qquad ++-\underbrace{0\cdots0}_{s_3}-,$$

and

$$-\underbrace{0\cdots0}_{s_3}-++, \qquad \text{and} \qquad +\underbrace{0\cdots0}_{s_3}+--. \qquad [27]$$

The amplitude of these segments is

$$\Lambda_{+,+}\Lambda_{+,-}\Lambda_{-,0}\Lambda_{0,0}{}^{s_3-1}\Lambda_{0,-}. \qquad [28]$$

These segments are in fact equivalent to those formed by a singly stimulated segment and triple echoes, for example, in Table 1, class 9. The addition diffusion decay compared to the parent triple echo is $2 s_3$.

Following the above discussion, one may continue to explore further classification of coherence segments with more complexity, for example, +'s and −'s inside a triple echo (Table 1, class 11) and more consecutive +'s and −'s (Table 1, class 15). We do not pursue it further here for the following reasons. The essence of our classification is to partition a CPMG coherence pathway into a few unique segments plus direct echo segments for the rest. These segments begin and end with the zero net phase. Since there are many types of such segments, our classification scheme quickly becomes very inefficient. We will show in the next section that the ones that we have discussed, in particular, the singly stimulated segments, dominate the echo signal.

IV. PERMUTATION, SPECTRUM, AND AMPLITUDE

A. Permutation: Counting Coherence Pathways

For $N_1 > 0$, there are many permutations of the stimulated and the direct echo segments for the same ηN. For instance, the value of N_1 determines the decay rate of all these pathways; however, different sets of n_{s_1} may have different amplitudes. For a given set of n_{s_1}, different permutations will result in identical matrix elements and thus amplitudes. Thus, in order to calculate the echo signal, such degeneracy needs to be evaluated, as listed in Table 1 for the fifth echo. For large N, the degeneracy is enormous.

Assume there are a series of different types of segments, $s_1 = 1$ to l, and that there are n_{s_1} segments for each s_1. Then, the number of possible permutations, provided all segments are

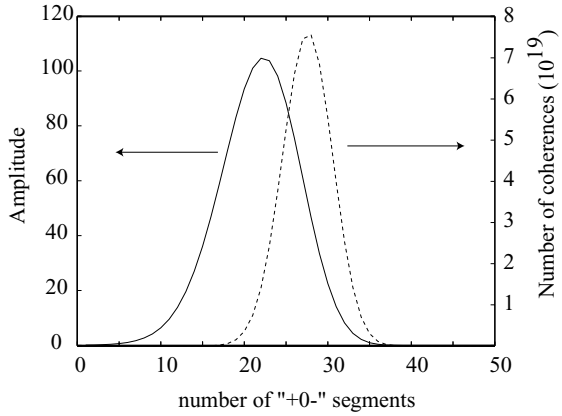

FIG. 1. Number of coherence pathways (dashed line) for the 100th echo formed by $-0+$ and direct echo segments and their amplitude contribution (solid line), as a function of the number of $-0+$'s, N_1. Many coherence pathways are contributing significantly to the echo signal and it is important to count them all. The amplitude is calculated using the asymptotic echo as a filter.

separated, is

$$U = \frac{(K-l)!}{(K-2l+1)!}\frac{1}{\prod_{i=1}^{l} n_i!}, \qquad [29]$$

where $K = N - \sum_{s_1=1}^{l}(s_1-1)n_{s_1}$. For the stimulated echo pathways, the matrix element decays as N increases. However, the number of possible permutations increases. For a given coherence pathway formed by several segments, U as a function of echo number N shows a broad peak and the peak position depends on the number of segments. In Fig. 1, we show the number of coherence pathways for the 100th echo formed by the simplest stimulated segments, $+0-$, as a function of the number of such segment n_1. As would be intuitively expected, maximum U occurs when n_1 is around 25–30. The contribution to the corresponding amplitude is also shown in Fig. 1.

B. Spectrum

Equation [8] determines the echo signal as a function of the frequency offset, $\Delta\omega_0$, or the spectrum. Because of the frequency dependence of the matrix elements, L and Λ, the decay due to diffusion in a field gradient is generally different at different frequencies. For example, with ideal $\pi/2$ and π pulses, the on-resonance signal contains only the direct echo pathway and the decay rate is given by the Hahn formula, $D(\gamma g t_e)^2/12$. However, the off-resonance signal has a much greater contribution from other coherence pathways, such as the stimulated ones, thus, the decay rate can be significantly higher.

In Fig. 2, we show a series of spectra of the singly stimulated coherence pathways for the 30th echo. The spectrum of the direct echo pathway ($s_1 = 0$) is concentrated at the resonance frequency, much narrower than those for the earlier echoes, as illustrated by Hürlimann (*12*). This is due to the finite bandwidth of the π pulse in inverting coherences from $+$ to $-$, and vice versa, e.g., $\Lambda_{+,-}$ and $\Lambda_{-,+}$. None of the stimulated coherence pathways contribute to the on-resonance signal, a result of the ideal π pulses. The spectra of these stimulated pathways are characterized by the two positive peaks at a nonzero $\Delta\omega_0$ and by their progressive movement further off-resonance for large N_1's. Around $\Delta\omega_0 = 0$, the spectra for most stimulated coherence pathways oscillate and the oscillations are out of phase for adjacent N_1's. Thus, a sum of two or more stimulated pathways with similar N_1 would result in a cancelation of the amplitude at small $\Delta\omega_0$. The result of such cancelation is shown in Fig. 2c illustrating that the off-resonance signal originates primarily from the stimulated coherence pathways. For a larger frequency offset, the signal comes from coherence pathways with larger N_1 containing more stimulated segments. In fact, one may take advantage of this property to determine a diffusion constant using just one CPMG echo train. Such behavior of the spectrum of the coherence pathways is unique for the high echo numbers. For the earlier echoes, illustrated in Fig. 8 of Ref. (*12*), the peaks in the spectrum of each coherence pathway are much broader than those for the high echoes, resulting in significant overlap of the spectra.

Using the spectrum for each coherence pathway, we have computed the average diffusion decay factor, $\eta N = N + 2N_1$ for

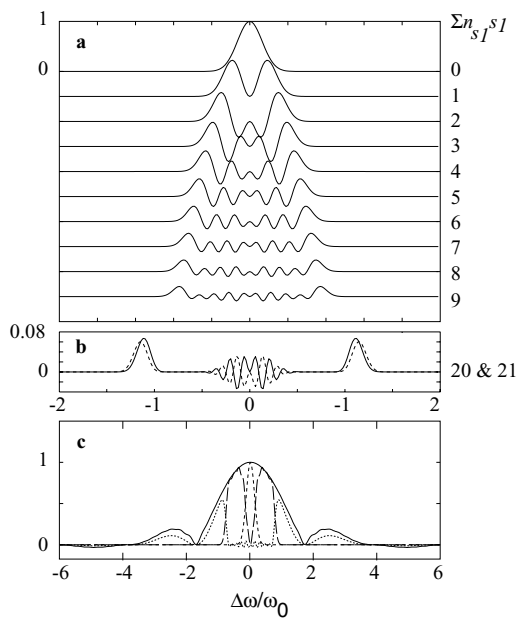

FIG. 2. (a, b) Spectra of some singly stimulated coherence pathways for the 30th echo listed by N_1. The direct echo contributes to primarily the on-resonance signal, and the stimulated coherence pathways contribute to off-resonance signals. The panel (b) displays the spectra for $N_1 = 20$ (solid line) and $N_1 = 21$ (dotted line). (c) Spectrum of the asymptotic echo (solid line), direct echo (short dashed line), sum of coherence pathways $N_1 = 1, 2, 3, 4, 5, 6, 7, 8, 9$ (long dashed line), and sum of pathways $N_1 = 10$ to 30 (dotted line). It is clear that the stimulated coherence pathways contribute to mainly the off-resonance signal.

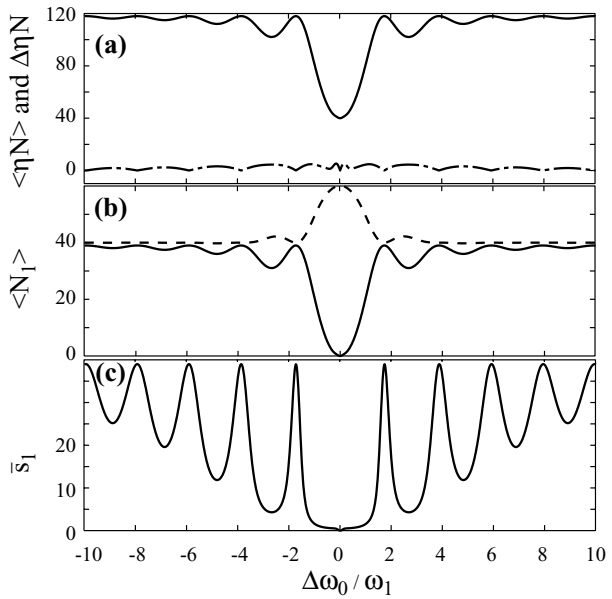

FIG. 3. (a) The average diffusion decay factor $\langle \eta N \rangle$ (solid line) and its variance $\Delta \eta N$ (dashed–dotted line) are shown as a function of frequency offset, $\Delta\omega_0$, for the 40th echo. (b) The average number of stimulated segments, $\langle N_1 \rangle$ (solid line), for the 40th echo, as a function of $\Delta\omega_0$. The spectrum is shown as the dashed line, and it is shifted for clarity. (c) The spectrum of the average segment length, $\bar{s}_1 \equiv \langle N_1 / \sum n_{s_1} \rangle$. Within the main peak, the average segment length is very small and the average segment length over the entire spectrum is 1.5 for the 40th echo.

the singly stimulated coherence pathways, displayed in Fig. 3a for $N = 40$. At $\Delta\omega_0 = 0$, the decay factor is 40, the result of the direct echo pathway. As $\Delta\omega_0$ deviates from zero, the decay factor increases to about a factor of three larger when $|\Delta\omega_0| > 1.5\omega_1$. The second moment of the ηN distribution is observed (Fig. 3a) to be very small, indicating that the decay at each $\Delta\omega_0$ is approximately exponential. This realization allows a straightforward analysis of the change of lineshape as a function of echo number. For example, these results can be used to construct an analytical function of the signal decay.

Furthermore, the narrow distribution of ηN indicates that at each frequency, the signal is dominated by a group of coherence pathways with a narrow distribution of N_1, since $\eta N = N + 2N_1$ for singly stimulated coherence pathways. Thus, one may obtain the average length of the stimulated segments as a function of $\Delta\omega_0$, Fig. 3b. Close to on-resonance, the average stimulated segment size is very small and the coherence pathways are dominated by the direct echo segments. At $\Delta\omega_0 \sim \omega_1$, N_1 is about $0.5N$ and half of the coherence pathways are stimulated, $q_k = 0$. For $\Delta\omega_0 > 2\omega_1$, $N_1 \sim N$ and there are very few direct echo segments and most of the segments are stimulated. We have performed similar calculations for the 30th, 40th, and 50th echoes and the above discussion is supported by the results for all three cases. This reaffirms that behavior of the 30th and higher echoes well approximates that of the asymptotic echo and the above conclusion is indeed valid for high echo numbers.

In Fig. 3c, we show the average segment length $\bar{s}_1$ as a function of $\Delta\omega_0$, for the 40th echo,

$$\bar{s}_1 \equiv \left\langle \frac{N_1}{\sum_{s_1=0}^{N_1} n_{s_1}} \right\rangle Q, \qquad [30]$$

averaged for all coherence pathways Q. Within the width of the main peak, $|\Delta\omega_0| < \omega_1$, $\bar{s}_1$ is less than 2, and the segment size averaged for the entire spectrum is 1.45. For the 50th echo, $\bar{s}_1 = 1.45$, too. This result indicates that the dominant coherence segments are $+-$, $+0-$, and $+00-$, and their variance and the long stimulated segments with large s_1 are not important even when N_1 can be as large as $N/2$ at $|\Delta\omega_0| \sim \omega_1$. We will further discuss this result later with regard to restricted diffusion.

C. Signal Amplitude

When one number is expected to represent the echo signal, it generally combines the signal at all frequencies. For example, one may take an integral of the echo in time domain corresponding to on-resonance, or the peak height corresponding to an integration in the frequency domain, or finite bandwidth can be applied in the detection (*8*). In general, one may assign a weighting function $w(\omega)$ to filter the echo signal,

$$A^N = \frac{\int d\omega M^N(\omega) w(\omega)}{[\int d\omega w^*(\omega) w(\omega)]^{1/2}}, \qquad [31]$$

where M^N is the spectrum for the Nth echo. We follow Ref. (*12*) to use the asymptotic echo spectrum as the filter $w(\omega)$ for optimal signal-to-noise ratio. In Fig. 4, we show the amplitude contribution from each coherence pathway for $N = 1$–14. This figure is similar to Fig. 12 in Ref. (*12*) except that the horizontal axis is linear in $\eta N - N$. The benefit of such an axis is that it allows a straightforward identification of the coherence pathways from such a diagram. For example, the position at $\eta N - N = 0, 2, 4, 6, \ldots$, corresponds to $N_1 = 0, 1, 2, 3, \ldots$ of the singly stimulated coherence pathways.

In Fig. 5, we show the amplitudes of the first 14 singly stimulated echoes (N_1 from 0 to 13). The decay of the direct echo is due to the off-resonance effects on the matrix element $\Lambda_{+,-}$ since there is only one direct echo pathway. It is intriguing to note that some of the coherence pathways have identical amplitudes for large N, for example, direct echo and $N_1 = 1$, and pathways with $N_1 = 2i$ and $2i + 1$ (i is an integer).

In the inset of Fig. 5, we show the sum of contributions from the direct echo and the singly stimulated pathways, as a function of N. For the first 20 echoes, one may observe that these two classes account for, on average, 95% of the echo signals. The amplitude oscillation for the early echoes decreases rapidly when N approaches 20. Beyond the 20th echoes, the contribution from the above coherence pathways decays gradually due to the effects of the matrix elements. Including more coherence pathways formed by the first 20 singly stimulated segments recovers

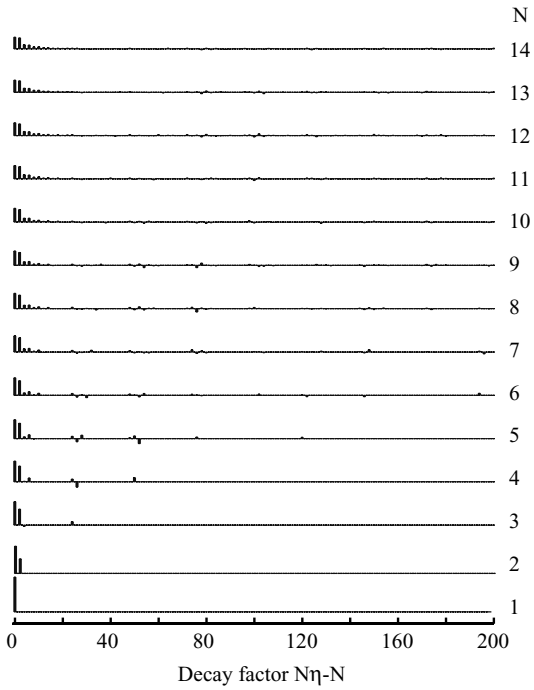

FIG. 4. Amplitude of individual coherence pathways for up to the 14th echo. The horizontal axis is $\eta N - N$ so that one can directly identify coherence pathways from this diagram. The pulses in the CPMG sequence are assumed to be accurate.

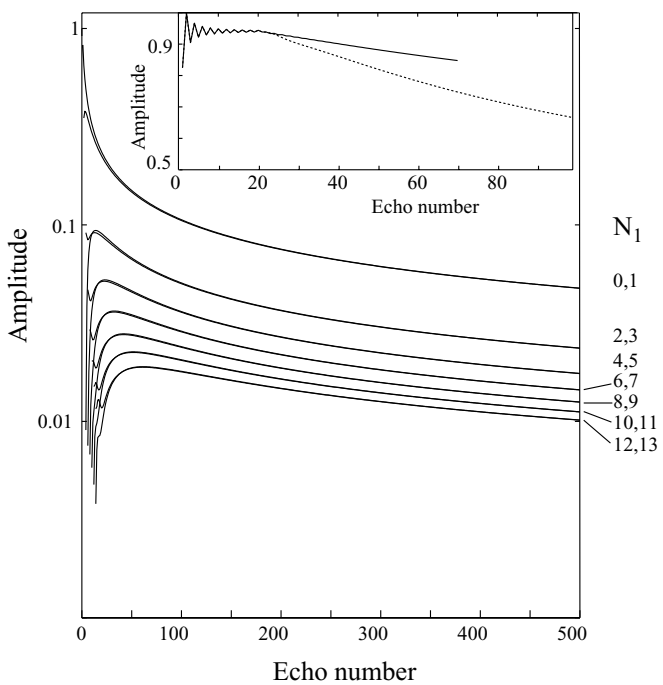

FIG. 5. Amplitudes of the first 13 singly stimulated echo segments as a function of echo number. Several negative amplitudes at the beginning of some pathways are neglected. The pulses in the CPMG sequence are assumed to be accurate. (Inset) Sum of the amplitudes of the direct echo and the first 20 singly stimulated segments as a function of echo number. The solid line includes all contributions from s_1 up to 20 and the dotted line includes only that with $N_1 \leq 20$.

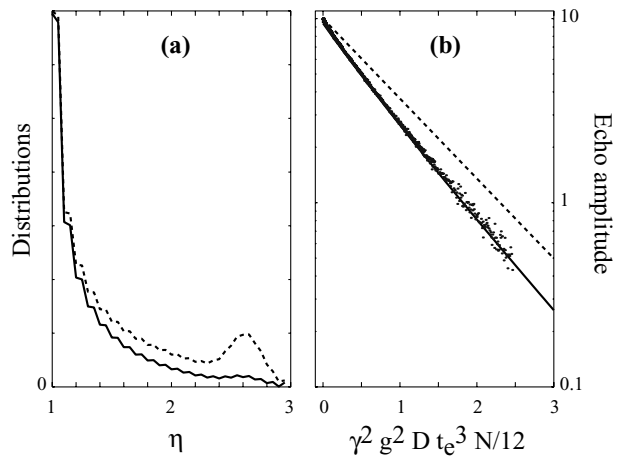

FIG. 6. (a) Amplitudes of the decay rate (η) distribution for the 40th echo. The distributions were calculated with asymptotic echo filtering (solid line) and without such filter (dashed line). (b) Echo amplitude as a function of $D\gamma^2 g^2 t_e^3 N/12$ for $N = 40$ (solid line). The dashed line is the decay for the on-resonance signal, i.e., the direct echo pathway. The points are data from Ref. (*12*) extending from $D\gamma^2 g^2 t_e^3 N/12 \approx 0$ to 2.5. The solid line is clearly a good match for the data except for a 5% error when $D\gamma^2 g^2 t_e^3 N/12 < 0.1$.

a portion of that amplitude. Nevertheless, this is still not a complete account of all singly stimulated segments. When all singly stimulated pathways are included, we obtain 0.942 for signals of the 30th, 40th, and 50th echoes.

After integration over the entire frequency spectrum using the asymptotic echo as a filter, we found that the average decay factor $\overline{\eta N} = 1.32N$, with a second moment of $(0.36N)^2$, for the 30th, 40th, and 50th echoes. This result suggests practical strategies to approximate the echo decay. To the lowest order of approximation when $\gamma^2 g^2 t_e^3 N/12 < 1$, the decay of CPMG echoes is a factor 32% faster than the Hahn formula. For $\gamma^2 g^2 t_e^3 N/12 > 1$, the decay is clearly multiexponential with a range of about 30% of the decay rate. The distribution of decay rate calculated from the spectra in Fig. 2 is shown in Fig. 6 for signals with and without the filter. Using the distribution, one may express the echo decay as a sum of a series of exponential functions

$$\frac{M(\alpha)}{M_0} = \exp(-\alpha) \cdot \left\{ a_0 + \sum_{l=1}^{40} a_l \exp\left(-\alpha \frac{2l}{40}\right) \right\}, \qquad [32]$$

where $\alpha \equiv D\gamma^2 g^2 t_e^3 N/12$ and a_l is given in Table 2 for the case of filtering. We note that the above formula has only one parameter α and can be directly used in an inversion algorithm. Equation [32] is compared with the experimental data reported in Ref. (*12*), in Fig. 6. The calculated decay curve fits very well the experimental data except for the 5% error when $\gamma^2 g^2 t_e^3 N/12 < 0.1$. This error is due to the fact that the singly stimulated pathways miss 5% of the signal. This error can be corrected empirically or by including more coherence segments such as triple echoes.

TABLE 2
Coefficients of the Decay Rate Distribution, a_l, for the 40th Echo with Asymptotic Echo Filtering

$a_0 = 0.1672$	$a_1 = 0.1633$	$a_2 = 0.0738$	$a_3 = 0.0724$
0.0490	0.0481	0.0360	0.0356
0.0279	0.0276	0.0221	0.0220
0.0178	0.0178	0.0145	0.0146
0.0118	0.0120	0.0097	0.0099
0.0079	0.0082	0.0064	0.0067
0.0052	0.0055	0.0042	0.0048
0.0038	0.0048	0.0042	0.0052
0.0044	0.0049	0.0034	0.0035
0.0017	0.0022	0.0002	0.0020

Note. The index increments along the row first, then column.

V. EFFECTS OF INACCURATE PULSES

When the RF pulses in CPMG are not accurately $\pi/2$ and π, certain aspects of the spin dynamics will be changed due to the matrix elements. Although the coherence pathways will remain the same, their weight will be different. For example, we can illustrate this effect using the on-resonance signal for the second echo. As the tipping angle $\omega_1 t_{180}$ deviates from π, the direct echo amplitude, $\propto \sin(\omega_1 t_{90}) \cos(\omega_1 t_{180})^2$, will decrease and that of the stimulated coherence pathways will increase from zero, $\propto \sin(\omega_1 t_{90}) \sin(\omega_1 t_{180})^2$. We show the results of similar calculations as those presented in early sections on ideal pulses in Fig. 7 for $\omega_1 t_{180} = 0.7\pi$ and the 40th echo. From these calculations, we have made the following observations:

- When the tipping angle deviates significantly from π, the $\Lambda_{+,-}$ is less than unity for all frequencies. Thus, the direct echo decays quickly and it has little contribution for large-N echoes. For example, in Fig. 7a, the spectrum for $N_1 = 0$ is essentially zero. The low N_1 coherence pathways show spectra that peaked at $\Delta\omega_0 = 0$, similar to the spectrum of the direct echo for ideal pulses. The amplitude of these low-N_1 spectra increases as N_1 and reaches a maximum at certain N_1 depending on $\omega_1 t_{180}$. The spectra for large N_1 are similar to their counterparts in the case of ideal pulses in that they have two peaks at off-resonance positions and their spectra near $\Delta\omega_0 = 0$ oscillates. Averaging the spectra with similar N_1's cancels such oscillations resulting in signals only at off-resonance frequencies.
- At all frequency offsets, the decay is approximately exponential, illustrated by the small second moments of the decay rate distribution shown in Fig. 7b. The rate at $\Delta\omega_0 = 0$ is also raised from its value for ideal pulses, a result of the stimulated pathways being the main contributors of the signal.
- Similar to the case of ideal pulses, the average segment length remains small within the width of the spectrum, Fig. 7c. Averaging over the entire spectrum, $\bar{s}_1 = 1.7$ for $\omega_1 t_{180} = 0.7\pi$, only increasing slightly from the case of ideal pulses (see Table 3).
- Due to the dominant contribution of the low-N_1 coherence pathways, the peak of the decay rate distribution moves to higher

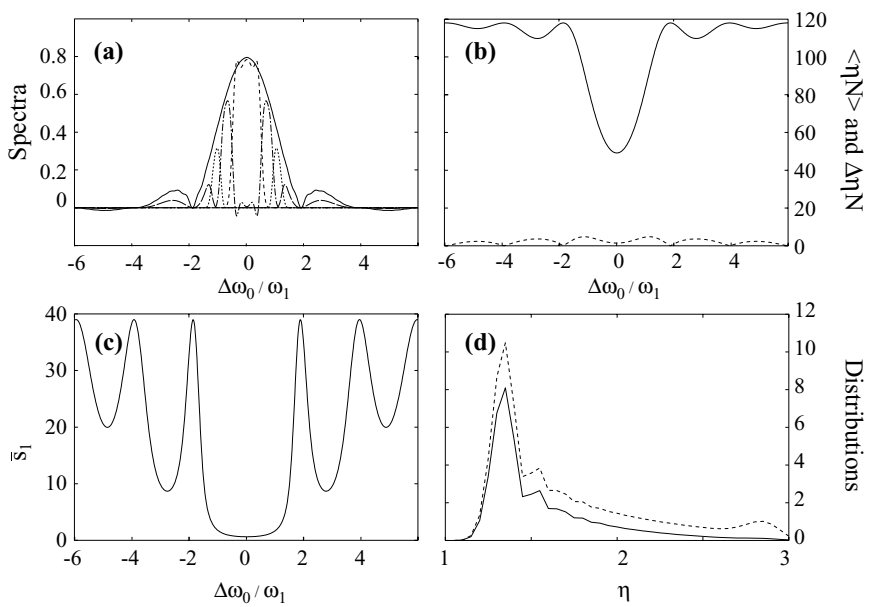

FIG. 7. The CPMG spin dynamics for the 40th echo with $\omega_1 t_{180} = 0.7\pi$. (a) Spectra of the asymptotic echo (solid line), sum of coherence pathways $N_1 = 1$–9 (dashed line), $N_1 = 10$–20 (dash-dotted line), $N_1 = 21$–29 (short dashed line), and $N_1 = 30$–40 (long dashed line). The signal of direct echo is essentially zero on this graph. (b) The average diffusion decay factor $\langle \eta N \rangle$ (solid line) and its variance $\Delta\eta N$ (dashed-dotted line) are shown as a function of frequency offset, $\Delta\omega_0$. (c) The spectrum of the average segment length, $\bar{s} \equiv \langle N_1 / \sum n_{s1} \rangle$. Within the main peak, the average segment length is very small and the average segment length over the entire spectrum is 1.71. (d) Amplitude of the decay rate (η) distribution. The distributions were calculated with asymptotic echo filtering (solid line) and without such filter (dashed line).

TABLE 3

The Average Decay Rate $\bar{\eta}$, Square-Root of the Second Moment of the η Distribution, $\Delta\eta$, and the Average Segment Length $\bar{s}_1$, Calculated for Several $\omega_1 t_{180}$

$\omega_1 t_{180}/\pi$	$\bar{\eta}$	$\Delta\eta$	$\bar{s}_1$
0.5	1.85	0.22	2.38
0.6	1.63	0.26	1.96
0.7	1.47	0.29	1.71
0.8	1.37	0.32	1.57
0.9	1.31	0.34	1.50
1	1.30	0.36	1.45

Note. This calculation uses the asymptotic echo spectrum as the filter function $w(\omega)$.

η, Fig. 7d, compared to the case of ideal pulses. The signal decay remains multiexponential; however, the range of η is reduced as the tipping angle deviates from π.

In these calculations, we have neglected the spatial variation of the RF field. To summarize, the main effects of the inaccurate RF pulses are the reduction of signal and the further increase of the decay rate.

VI. RELATIONSHIP TO *k*-SPACE FORMALISM

In MRI and NMR experiments using magnetic field gradients, it is often convenient to use a wave vector (often noted as **k** or **q**) to describe the spatial modulation of the magnetization and its change in a manner similar to the description of scattered waves (*6, 19, 22–24*). In this scheme, the progress of the wave vector in an experiment is usually illustrated in a one-dimensional or two-dimensional diagram depicting the effects of the gradients and RF pulses in changing the modulation. Each particular passage of **k** to the final echo signal corresponds to a coherence pathway described in this paper. The two descriptions are, in fact, equivalent and the coherence pathways can be easily mapped onto the **k**-space formalism by defining $\mathbf{k}(T) = \int_0^T \gamma g q(t)\, dt$. Here, $q(t)$ is the continuous version of q_k used in earlier sections. We will define $\mathbf{k}_0 = \gamma g t_e/2$ as the unit, which is the value before the first π pulse. The direct echo pathway corresponds to a **k** trajectory zigzagging around the origin between $\mathbf{k} = +\mathbf{k}_0$ and $\mathbf{k} = -\mathbf{k}_0$. The singly stimulated segments correspond to **k** rises to $\pm\mathbf{k}_0$, then stay at that value for a time period of $s_1 t_e$ before coming back to $\mathbf{k} = 0$. In fact, the entire ensemble of the singly stimulated coherence pathways are **k** trajectories that stay completely within $\pm\mathbf{k}_0$. Similarly, the triple echo and triply stimulated segments are those trajectories entering the domains of $[\mathbf{k}_0, 3\mathbf{k}_0]$ or $[-3\mathbf{k}_0, -\mathbf{k}_0]$. Thus, the conclusion from earlier sections that the direct and singly stimulated echoes are the dominant contribution to CPMG signals can be visualized as those wave-vector trajectories that do not deviate much from the line of no modulation, i.e., $\mathbf{k} = 0$.

VII. EFFECT OF RESTRICTED DIFFUSION

It is well known that molecular diffusion is restricted in porous media due to the confinement of the pore space (*25*). One of the most widely used approaches is the concept of time dependent diffusion constant, $D(t)$ (*20, 25*)

$$D(t) \equiv \frac{\langle r^2 \rangle}{6t}, \qquad [33]$$

where t is the diffusion time and $\langle r^2 \rangle$ is the mean-square displacement. For diffusion in bulk fluid, $D(t)$ is a constant in time, since $\langle r^2 \rangle = 6Dt$. In porous media, $D(t)$ will be reduced from the bulk value when $\sqrt{Dt}$ is close to the geometrical length scales of the pores, such as the inverse of the surface-to-volume ratio and the linear dimension (*26–29*). This behavior has been observed a wide range of porous media using pulsed-field gradients (PFG) NMR methods (*19*). In a PFG experiment, the diffusion time can be easily determined from the pulse sequence. However, in a CPMG experiment, it is not obvious from the pulse sequence directly what the diffusion time should be and what diffusion constant should be used. Previous works (*15, 21, 30*) have focused on the direct echo pathway and showed that the diffusion time for this pathway should be on the order of t_e. On the other hand, coherence pathways with large s_1 could necessitate the use of a long time diffusion constant, i.e., $D(s_1 t_e)$. It has been unclear whether these high s_1 pathways could have a significant contribution to the CPMG echoes.

Previous works, such as Refs. (*8, 12*), have shown that the stimulated segments have a significant contribution to the signal. Our analysis of the spectra for different pathways in earlier sections indicates that these stimulated segments increase the average decay rate by 32% compared to the Hahn formula. Furthermore, we found that the dominant contribution is from those coherence pathways with very short segments and $\bar{s}_1$ remains very small, $\bar{s}_1 = 1.45$–1.85 for a wide range of tipping angles. The average time scale that governs the diffusion decay is approximately $(\bar{s}_1 + 1/3)t_e < 2.2t_e$. Thus, the inclusion of the additional coherence pathways in the off-resonance signals does not extend significantly the diffusion time scale compared to that of the direct echo. As a result, the effects of restricted diffusion and the characteristic regimes outlined by Sen *et al.* in Refs. (*15, 21, 30*) based on the direct echo pathway are in principle applicable to the off-resonance signals of CPMG.

VIII. CONCLUSIONS

This paper outlines a scheme to understand the CPMG coherence pathways and the effect of molecular diffusion by breaking up the CPMG coherence pathways into small and simple segments. We found that the direct echo and the stimulated segments are most abundant and contribute about 95% of the CPMG echo signal. Inclusion of such coherence pathways in the detection

could increase the average decay rate by 32%. For the Nth echo, there will be on average $0.16N$ segments of $q = 0$. These coherence pathways are predominantly constituted of short segments with an average segment length of $1.5t_e$.

These observations suggest that despite the enormously large variety of the contributing pathways, a conceptual understanding of CPMG remains quite simple. There is a fundamental repeating unit of the coherence and it is only slightly expanded from that of the Hahn echo coherence pathway.

Furthermore, these results are relevant for applications of the CPMG sequence especially to materials made of multiple components of relaxation and diffusion. For example, we show that one has to calibrate the detection scheme as well as the RF strength in order to account quantitatively for the enhanced decay rates. We have provided an analytical form for the CPMG echo decay (Eq. [32]) that could be used as a kernel function to invert for the distribution of the diffusion constants from single and multiple CPMG echo trains.

ACKNOWLEDGMENTS

The author acknowledges discussions with L. Zielinski P. N. Sen, M. D. Hürlimann, D. Freed, and D. G. Cory. The author also thanks M. D. Hürlimann for the use of his computer program for Fig. 4.

REFERENCES

1. H. Y. Carr and E. M. Purcell, Effects of diffusion on free precession in NMR experiments, *Phys. Rev.* **94,** 630 (1954).
2. S. Meiboom and D. Gill, Compensation for pulse imperfections in Carr–Purcell NMR experiments, *Rev. Sci. Instrum.* **29,** 688 (1958).
3. R. Kleinberg, *in* "Encyclopedia of Nuclear Magnetic Resonance" (D. M. Grant and R. K. Harris, Eds.), Wiley, New York (1995).
4. P. J. McDonald, Stray field magnetic resonance imaging, *Prog. Nucl. Magn. Reson. Spectrosc.* **30,** 69 (97).
5. G. Eidmann, R. Savelsberg, P. Blümler, and B. Blümich, The NMR mouse, a mobile universal surface explore, *J. Magn. Reson. A* **122,** 104 (1996).
6. J. Hennig, Multecho imaging sequences with low refocusing flip angles, *J. Magn. Reson.* **78,** 397 (1988).
7. R. Kaiser, E. Bartholdi, and R. R. Ernst, Diffusion and field-gradient effects in NMR Fourier spectroscopy, *J. Chem. Phys.* **60,** 2966 (1974).
8. G. Goelman and M. G. Prammer, The CPMG pulse sequence in strong mangetic field gradients with applications to oil-well logging, *J. Magn. Reson. A* **113,** 11 (1995).
9. J. Simbrunner and R. Stollberger, Analysis of Carr–Purcell sequences with nonideal pulses, *J. Magn. Reson. B* **109,** 301 (1995).
10. A. Ross, M. Czisch, and G. C. King, Systematic errors associated with CPMG pulse sequence and their effect on motional analysis of biomolecules, *J. Magn. Reson.* **124,** 355 (1997).
11. F. Bălibanu, K. Hailu, R. Eymael, D. E. Demco, and B. Blümich, Nuclear magnetic resonance in inhomogeneous magnetic field, *J. Magn. Reson.* **145,** 246 (2000).
12. M. D. Hürlimann, Diffusion and relaxation effects in general stray field NMR experiments, *J. Magn. Reson.* **148,** 367 (2001).
13. J. E. Tanner and E. O. Stejskal, Restricted self-diffusion of protons in colloidal systems by the pulsed-gradient, spin-echo method, *J. Chem. Phys.* **49,** 1768 (1968).
14. P. T. Callaghan, Pulsed-gradient spin-echo NMR for planar, cylindrical and spherical pores 24 under conditions of wall relaxation, *J. Magn. Reson. A* **113,** 53 (1995).
15. P. N. Sen, A. Andre, and S. Axelrod, Spin echoes of nuclear magnetization diffusing in a constant magnetic field gradient and in a restrict geometry, *J. Chem. Phys.* **111,** 6548 (1999).
16. E. L. Hahn, Spin echoes, *Phys. Rev.* **80,** 580 (1950).
17. D. E. Woesner, Effects of diffusion in nuclear magnetic resonance spin-echo experiments, *J. Chem. Phys.* **34,** 2057 (1961).
18. E. O. Stejskal and J. E. Tanner, Spin diffusion measurements: Spin echoes in the presence of a time-dependent field gradient, *J. Chem. Phys.* **42,** 288 (1965).
19. P. T. Callaghan, "Principles of Nuclear Magnetic Resonance Microscopy," Oxford Univ. Press, New York (1993).
20. P. P. Mitra, P. N. Sen, L. M. Schwartz, and P. L. Doussal, diffusion propagator as a probe of the structure of porous media, *Phys. Rev. Lett.* **24,** 3555 (1992).
21. T. M. de Swiet and P. N. Sen, Decay of nuclear magnetization by bounded diffusion in a constant field gradient, *J. Chem. Phys.* **100,** 5597 (1994).
22. P. Mansfield and P. K. Grannell, "Diffraction" and microscopy in solids and liquids by NMR, *Phys. Rev. B* **12,** 3618 (1975).
23. T. R. Saarinen and C. S. Johnson, Jr., Imaging of transient magnetization gratings in NMR: Analogies with Laser-induced gratings and applications to diffusion and flow, *J. Magn. Reson.* **78,** 257 (1988).
24. A. Sodichson and D. G. Cory, A generalized k-space formalism for treating the spatial aspects of a variety of NMR experiments, *Prog. NMR Spectrosc.* **33,** 77 (1998).
25. D. E. Woessner, NMR spin-echo self-diffusion measurements on fluids undergoing restricted diffusion, *J. Phys. Chem.* **67,** 1365 (1963).
26. L. L. Latour, P. P. Mitra, R. L. Kleinberg, and C. H. Sotak, Time-dependent diffusion coefficient of fluids in porous media as a probe of surface-to-volume ratio, *J. Magn. Reson. A* **101,** 342 (1993).
27. M. D. Hürlimann, K. G. Helmer, L. L. Latour, and C. H. Sotak, Restricted diffusion in sedimentary rocks: Determination of surface-to-volume ratio and surface relaxivity, *J. Magn. Reson. A* **111,** 169 (1994).
28. L. L. Latour, P. P. Mitra, R. L. Kleinberg, and C. H. Sotak, Pore size distributions and tortuosity in heterogeneous porous media, *J. Magn. Reson. A* **112,** 83 (1995).
29. K. G. Helmer, B. J. Dardzinski, and C. H. Sotak, The application of porous-media theory to the investigation of time-dependent diffusion in in vivo systems, *NMR Biomed.* **8,** 297 (1995).
30. L. J. Zielinski and P. N. Sen, Relaxation of nuclear magnetization in a nonuniform magnetic field gradient and in a restricted geometry, *J. Magn. Reson.* **147,** 95 (2000).